Electronic Supplementary Material (ESI) for Physical Chemistry Chemical Physics.
This journal is © the Owner Societies 2023

Electronic Supplementary Information:

Solvent polarity dependence of ultrafast excited state dynamics of *trans*-4-nitrostilbebe

Peng-Yun Wang, Yu-Cheng Hsu, Pin-Hsun Chen, Guan-Yu Chen, Yi-Kai Liao, and Po-Yuan Cheng*

Department of Chemistry, National Tsing Hua University, Hsinchu, Taiwan 30043, R.O.C

*To whom correspondence should be addressed. E-mail: pycheng@mx.nthu.edu.tw

S1. Experimental

(1) Ultrafast broadband time-resolved fluorescence spectroscopy with optical Kerr gating

The home-built ultrafast broadband time-resolved fluorescence (TRFL) spectrometer used in this work is based on the optical Kerr gating technique.[1-3] The laser pulses were derived from a femtosecond laser system consisting of a self-mode-locked Ti:sapphire laser (Spectra Physics, Tsunami) and a 1 kHz chirped-pulse regenerative amplifier (CPA; Spectra Physics, Spitfire). A fraction of the CPA output at 766 nm (~120 fs FWHM) was frequency doubled to produce the excitation pulse at 383 nm. Alternatively, the major portion of the CPA output at 800 nm was used to pump an optical parametric amplifier (OPA, Light Conversion, TOPAS-C). The signal output of the OPA at 1440 nm was frequency doubled twice successively in two thin BBO crystals to produce excitation pulses at 360 nm. The remaining portion of the fundamental beam (766 nm or 800 nm) was used as the gate pulse.

The Kerr shutter consists of a Kerr medium (0.5-mm-thick liquid benzene) placed between a pair of crossed wire-grid polarizers (Moxtek, PPL04C). The excitation pulse was focused to excite sample solutions contained in a 2”-diameter rotating cell with an internal path length of 0.5 mm between a pair of 1-mm-thick fused silica window. A half-wave plate was used to rotate the excitation-laser polarization at the “magic angle” with respect to the first polarizer of the Kerr shutter. The fluorescence was collected by a 90° off-axis 2”-diameter parabolic mirror (effective f=75 mm) and was then directed through the first polarizer and focused on the Kerr medium by a second 90° off-axis parabolic mirror (effective f=150 mm). The gate pulse was directed through a computer-controlled delay line and then steered and focused to spatially overlap with the fluorescence spot at the Kerr medium. The polarization of the gate pulse was rotated by 45° with respect to the first polarizer to maximize for the gating efficiency.[1-3] Typical pulse energies used here were ~1-2 μJ/pulse for excitation and ~50-70 μJ/pulse for gating.

The gated fluorescence was collected and imaged onto the entrance slit of a spectrograph (Andor, SR163, 300 lines/mm grating) via a pair of achromatic lenses. The entrance slit was adjusted to give an effective bandpass (fwhm) of about 6 nm. A long-pass filter (Schott GG-400) and a short-pass filter (Omega Optical 728SP) filter were placed in front of the spectrograph entrance slit to reject the scattered light, limiting the detection spectral range to

be ~400 nm-720 nm. The dispersed fluorescence spectra were recorded by A TE-cooled CCD camera (Andor, DU970N-BV). In TRFL experiments presented here, the combination of the CCD camera "binning" and the spectrograph bandpass resulted in an effective spectral resolution of ~6 nm as estimated from solvent Raman lines. A computer program was devised to automate the data acquisition. The program stops the translation stage at a series of pre-selected positions and records the gated fluorescence spectra at the corresponding delay times. A background spectrum taken at a negative delay time (usually at -20 ps) at the beginning of each scan was subtracted from the spectra measured at other delay times. The program records TRFL spectra at the preselected delay times and averaged by scanning the translation stage back and forth until a satisfactory signal-to-noise (S/N) ratio is achieved. The TRFL spectra are corrected for spectral sensitivity and temporal dispersion using procedures that have been described in our previous report.[4]

The temporal instrument response function (IRF) of the system described above can be obtained by measuring the Raman response of a pure solvent. The time trace of such measurement can be fitted with a model function consisting of a linear combination of a Gaussian and a reversed exponential decay function. A typical IRF time trace measured with the present setup is shown in Fig. S1, and the full width at half maximum (FWHM) of the effective IRF is 0.34±0.02 ps. The model function thus obtained was then used as the temporal IRF for fitting fluorescence transients and total fluorescence intensity time traces (*P*(t)) using an iterative reconvolution nonlinear least square fitting procedure. Steady-state fluorescence

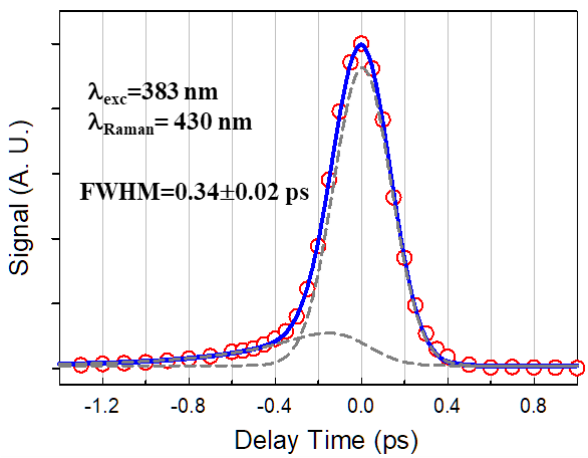

Fig. S1 A typical temporal IRF obtained by measuring the temporal response of Raman signal of a neat cyclohexane solvent (0.5 mm thick) with the ultrafast TRFL spectrometer described here. The solid line is the best fit of the data points (open circles) to a model function consisting of a Gaussian function and a reversed exponential decay (dashed lines).

spectra were recorded using the same setup described above for the TRFL experiments with both Kerr-shutter polarizers and the short-pass filter removed.

(2) Ultrafast broadband visible transient absorption (vis-TA) spectroscopy

The home-built ultrafast visible broadband transient absorption spectrometer used in this work employs a dual-beam configuration with single-shot spectral referencing. The pump pulses are produced in the same manner as in the TRFL experiments. A small fraction of the CPA output was directed through a computer-controlled optical delay line and then focused into a 3-mm cell containing pure water to produce the white-light continuum (WLC) pulse. The WLC pulse was recollimated with a 90° parabolic mirror and was sent into a 1 mm-pathlength cuvette containing an aqueous solution of $CuSO_4$ (~0.75 M) that acts as an optical filter to reduce the intensity of residual fundamental at 766 nm (or 800 nm). After passing a thin wire-grid polarizer, the resulting WLC pulse was then split into a probe and a reference pulses via an optical wedge. The probe and reference pulses were focused at the sample cell and directed into a pair of fiber-coupled photodiode array spectrometers (Avantes, AvaSpec-128, 300 l/mm grating, 50 μm slit, effective bandpass (fwhm)≈6 nm) using two identical sets of off-axis parabolic mirrors. The pump pulse was focused at ~2 cm behind the sample cell by a f= 500 mm CaF_2 lens and spatially overlapped with the probe pulse at the sample cell. The pump-laser polarization was rotated at the "magic angle" with respect to that of the WLC probe pulse with a half-wave plate. The two spectrometers record the WLC spectra of each probe and reference pulses, and a synchronized optical chopper (Thorlabs, MC1000) chops the pump beam such that individual 'pump-on' and 'pump-off' spectra can be separately recorded and stored in an on-board memory for data transferring. The transient absorption spectrum ($\Delta A(\lambda,t)$), i.e., the change in the sample absorbance induced by the pump pulse, at delay time t is calculated using the following expression,

$$\Delta A(\lambda,t) = -\log\left(\frac{I_P^*(\lambda,t)/I_R^*(\lambda)}{I_P^\circ(\lambda)/I_R^\circ(\lambda)}\right), \qquad \text{Eq. (S1)}$$

, where $I_P(\lambda)$ and $I_R(\lambda)$ are the probe and reference spectra, respectively, and the superscripts denote that the pump pulse was on (*) or off (°) at the corresponding shot. The optical chopper is normally run at 500 Hz to block every-other pump pulse to facilitate single-shot referencing.

At each preselected delay time in a scan, TA spectra are calculated using acquired spectra of consecutive shots and averaged over 1000-2000 shots. Alternatively, the optical chopper runs at 250 Hz and the spectrometers integrate two adjacent shots for pump-on and pump-off spectra. In this double-shot referencing scheme, the time needed to transfer data from the on-board memory to computer is reduced by a factor of two with a slight trade off in S/N ratio.

A background pure-solvent response is recorded under the same condition immediately after the TA measurement of a sample solution, and the transient 'artifacts' due to various nonlinear processes are removed by subtracting the background signal using the procedure suggested by Lorenc et al.[5] To correct for the temporal group delay dispersion, we first measured a wavelength-dependent time-zero curve of the probe WLC pulse with respect to the pump pulse with optical Kerr gating. To this end, a second wire-grid polarizer is placed in the probe beam path after the rotating cell with its transmission axis rotated at 90° with respect to that of the first one. A pure solvent loaded in the cell (same pathlength) is used as a Kerr medium, and the excitation pulse now acts as the gating pulse. By monitoring the gated WLC signal, the time zero at each probe wavelength can be accurately determined under the same condition of the TA experiment. To correct for the temporal dispersion in TA data, the TA time traces at each probe wavelength are first interpolated using a cubic spline algorithm and are then time-shifted according to the corresponding time-zero dispersion curve. The temporal IRF of the system can be measured in the same manner by replacing the sample cell with a

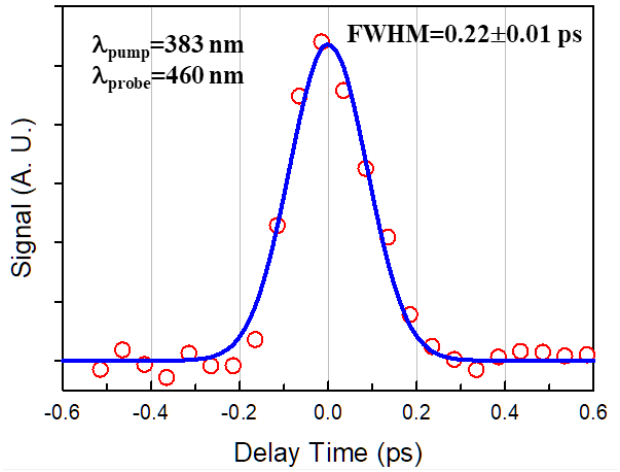

Fig. S2 A typical temporal IRF trace measured with the TA spectrometer modified to measure the OKG signal. It is done by replacing the sample cell with a 1mm-thick fused silica plate to act as a Kerr medium and placing a second wire-grid polarizer in the probe beam path after the fused silica plate with its transmission axis rotated at 90° with respect to that of the first one.

1mm-thick fused silica plate to act as the Kerr medium. The measured temporal IRF of the present setup can be well fitted to a Gaussian function with a FWHM of 0.22±0.01 ps, as shown in Fig. S2.

In both TRFL and TA experiments, results of each repetitive scan were also saved for latter inspections of any sign of sample degradation. This capability has proved to be particularly important in the present study of *t*-NSB which exhibits a high photoisomerization yield. Because of the limited volume of solution contained in the rotating cell, signal reduction and/or additional temporal/spectral features due to formation of photoproducts do appear in a relatively short data-acquisition timespan in the present case. By inspecting the data of each scan, data accumulated prior to the appearance of photo-induced degradation can be extracted and averaged for further analyses.

S2. Evaluation and Analyses of the time-dependent mean emission frequency ($\bar{\nu}(t)$)

The measured TRFL spectra after spectral-sensitivity and time corrections, $I'(\lambda,t)$, were first converted to frequency scale using $I(\nu) = I'(\lambda)\cdot\lambda^2$. The time-dependent mean emission frequency was then evaluated with

$$\bar{\nu}(t) = \frac{\int \nu \cdot I(\nu,t)d\nu}{\int I(\nu,t)d\nu} \qquad \text{Eq. (S2)}$$

, where $I(\nu, t)$ represents the TRFL spectra in frequency after spectral-sensitivity and time corrections. The time-dependent fluorescence dynamic Stokes shift (TDFSS) is defined as $\delta\bar{\nu}(t) = \bar{\nu}(t) - \bar{\nu}(\infty)$. The evaluations of $\bar{\nu}(t)$ require integrations over entire fluorescence spectral range. To this end, experimental TRFL spectra are fitted to a log-normal function of the form

$$g(\nu) = A \cdot \exp\left\{(-\ln 2)\left(\frac{\ln(1+\alpha)}{\gamma}\right)^2\right\}, \qquad \alpha \geq -1$$

$$= 0 \qquad , \qquad \alpha < 1 \qquad \text{Eq. (S3)}$$

$$\alpha = 2\gamma(\nu - \nu_p)/\Omega$$

, where ν_p is the peak frequency, Ω is the width parameter, and γ is the asymmetry parameter. The evaluation of $\bar{\nu}(t)$ was then performed with the results obtained from the log-normal

function fittings. Fig. S3(a) shows $\bar{\nu}(t)$'s of TRFL spectra of *t*-NSB in ACN, ACT, and TRA solvents obtained by using the procedure described above.

To extract time constants involved in $\bar{\nu}(t)$, we employed a deconvolution procedure suggested by Gutavaason et al.[6] Briefly, a new function $f(t)=J(t)\ \delta\bar{\nu}(t)$, where $J(t)=\int I(\nu,t)d\nu$, was calculated using the results from the lognormal-function fittings. $J(t)$ is simply the time dependence of the total fluorescence intensity. f(t) was then fit with the product of two multiple-exponential model functions, $J^*(t)\,\delta\bar{\nu}^*(t)$, convoluted with the IRF using an iterative reconvolution procedure. $J^*(t)$ is the deconvoluted function of $J(t)$ and can be obtained from fitting J(t) with a multiple-exponential model function. $\delta\bar{\nu}^*(t)$ is the deconvoluted function of $\delta\bar{\nu}(t)$ to be obtained from fitting f(t). The desired deconvoluted function of $\bar{\nu}(t)$ was then obtained by adding the relaxed mean emission frequency to $\delta\bar{\nu}^*(t)$, i.e., $\bar{\nu}^*(t)=\delta\bar{\nu}^*(t)+\bar{\nu}(\infty)$. The results of these fittings are shown in Figure S3(b) for *t*-NSB in ACN and ACT.

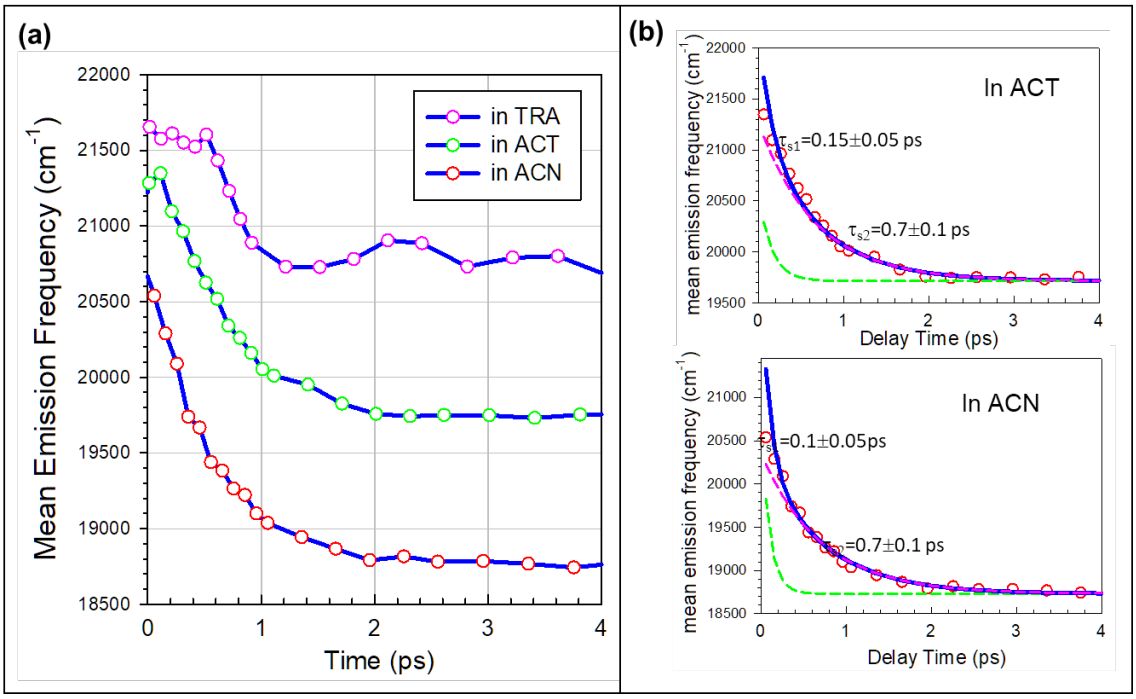

Fig. S3 (a) Time-dependent mean emission frequency ($\bar{\nu}(t)$) evaluated from TRFL spectra of *t*-NSB in ACN, ACT, and TRA solvents. Open circles are the evaluated data points and the interconnected lines are guides to the eye. (b) Fitting of $\bar{\nu}(t)$ data using the procedure described in **S2** for *t*-NSB in ACN and ACT data.

S3. Assessments of various density functionals for vertical excitation energies of *t*-NSB

We first assessed several popular functionals for their accuracies in predicting the first electronic absorption band maxima in both nonpolar (CHX) and polar (ACN) solvents. In these assessment calculations, the optimized ground-state structures of *t*-NSB in CHX and ACN solvents were calculated using the following functionals, PBE0, M06HF, wB97XD, MN15, and CAM-B3LYP, with the same basis set (cc-pVTZ). Solvation effects were included with the SMD variant of the polarizable continuum model using the integral equation formalism (IEFPCM) as implemented in the Gaussian 16 program.[7] Vibrational frequency calculations were performed to ensure each optimized structure corresponds to a true minimum at the level of theory used. Single-point vertical excitation energies of the first two singlet excited states, S_1 and S_2, in CHX and ACN solvents were then calculated with time-dependent (TD) DFT method with the same functional used to optimized the *t*-NSB ground-state structure. The calculated vertical excitation energies are listed in Table S1 as their corresponding wavelengths along with the experimental values for comparisons. Except for M06HF, all other functionals predict that the S_1 state to be the initial bright state in the first absorption band region. The S_2 state lying at a slightly higher energy is a dark state with a vanishing oscillator strength. Among all functionals, CAM-B3LYP gives results that are most consistent with the absorption maximum wavelengths observed in nonpolar CHX and highly-polar ACN solvents.

Table S1. Calculated vertical excitation wavelengths (in nm) from the S_0 state to the S_1 and S_2 states at the optimized S_0-state structure of *t*-NSB in CHX and ACN solvents.

	in CHX		in ACN	
functional	S_1	S_2	S_1	S_2
PBE0	376.1[a] (1.06)[b]	314.0 (0.00)	411.0 (1.23)	313.0 (0.00)
M06HF	316.0 (0.00)	294.3 (1.26)	315.2 (0.00)	310.2 (1.46)
ωB97XD	325.4 (1.24)	305.0 (0.00)	347.7 (1.42)	304.4 (0.00)
MN15	352.6 (1.14)	333.8 (0.00)	381.3 (1.31)	332.5 (0.00)
CAM-B3LYP	332.0 (1.21)	305.0 (0.00)	356.7 (1.38)	304.5 (0.00)
exp. λ_{abs}^{max} [c]	340 nm		351 nm	

[a]Calculated vertical excitation wavelengths in nm. [b]The values in parentheses are the corresponding oscillator strengths. [c]Experimental absorption maximum wavelength of the first UV-vis absorption band of *t*-NSB.

S4. Kinetic Modeling

The competing relaxation mechanism for the initially excited $S_1(\pi\pi^*)$ state in medium-polarity solvent described in Section 4.3 and Fig. 9(a) can be rearranged to the kinetic model shown below.

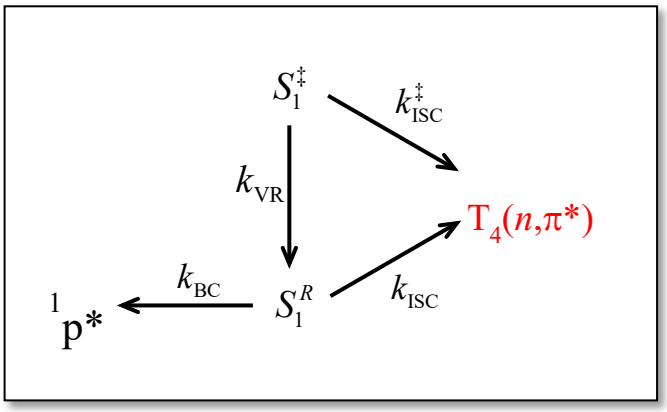

The time-dependent total fluorescent S_1-state population is

$$S_1^{total}(t) = S_1^{\ddagger}(t) + S_1^R(t)$$

, where $S_1^{\ddagger}(t) = S_1^{\ddagger}(0)e^{-k_1 t}$ and $S_1^R(t) = S_1^{\ddagger}(0)\dfrac{k_{\mathrm{VR}}}{k_1 - k_2}\left(e^{-k_2 t} - e^{-k_1 t}\right)$

, in which

$$k_1 = k_{\mathrm{ISC}}^{\ddagger} + k_{\mathrm{VR}}$$

$$k_2 = k_{\mathrm{ISC}} + k_{\mathrm{BC}}$$

For the fitting results shown in Fig. 9(b) we assumed that the emission transition moments of the $S_1^{\ddagger}$ and S_1^R states are the same and that $k_{\mathrm{BC}} = 0$.

S5. Other Supplementary Figures

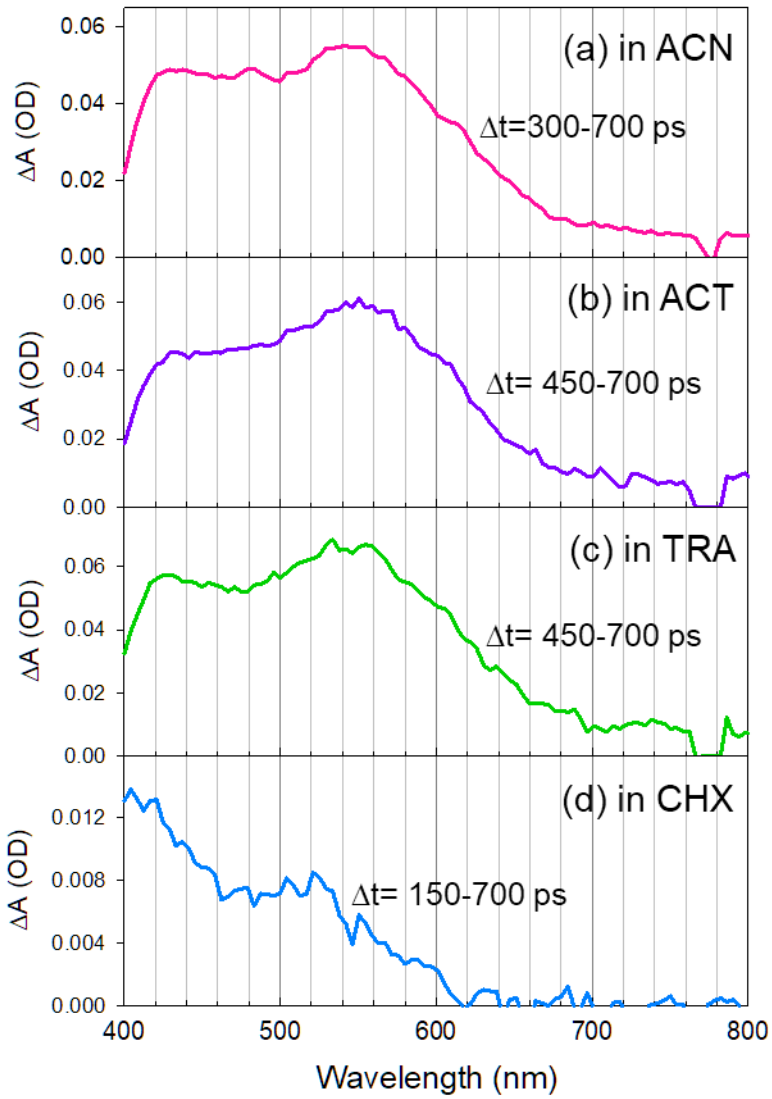

Fig. S4 Averaged long-lived ESA spectra of *t*-NSB in (a) ACN, (b) ACT, (c) TRA, and (d) CHX. These spectra are obtained by averaging TA spectra within the specified time ranges (Δt) within which TA signals remain nearly constant and can be assigned to the $T_1 \rightarrow T_n$ absorption.

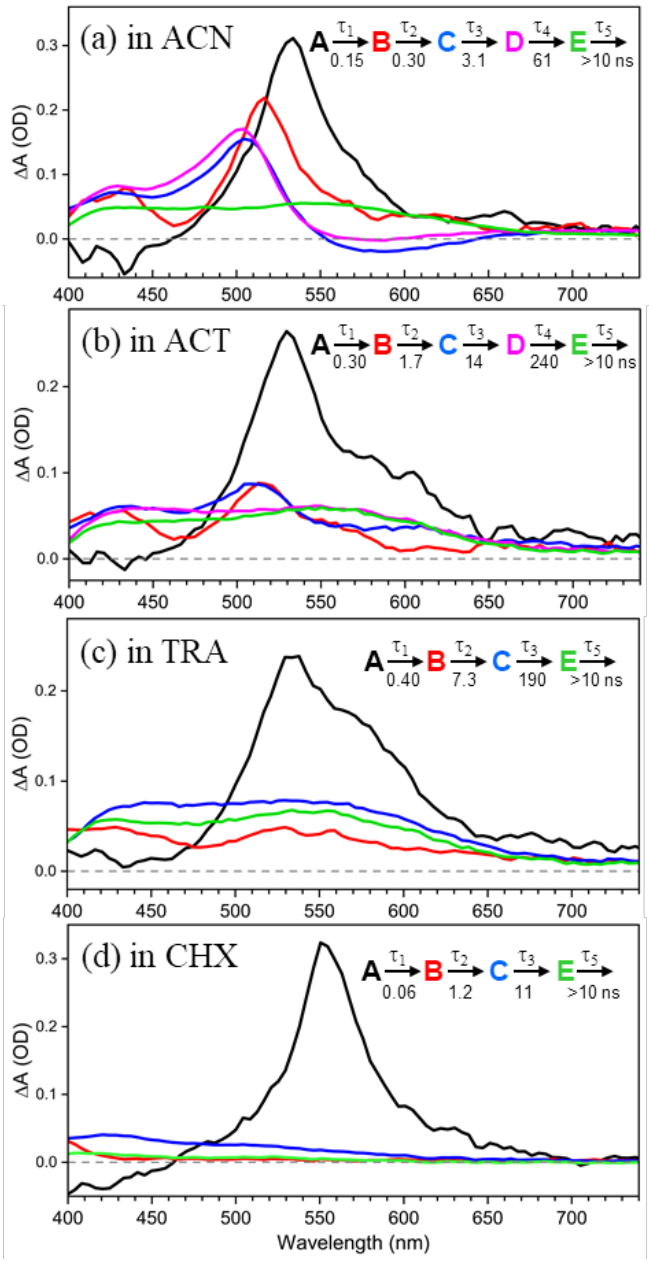

Fig. S5 Evolution-associated difference spectra (EADS) obtained from global fitting of the *t*-NSB TA data measured in four solvents with sequential reaction models of five or four steps. The corresponding time constants (in ps) of each step obtained from the fits are listed in Table 2 in the main text and are also shown here.

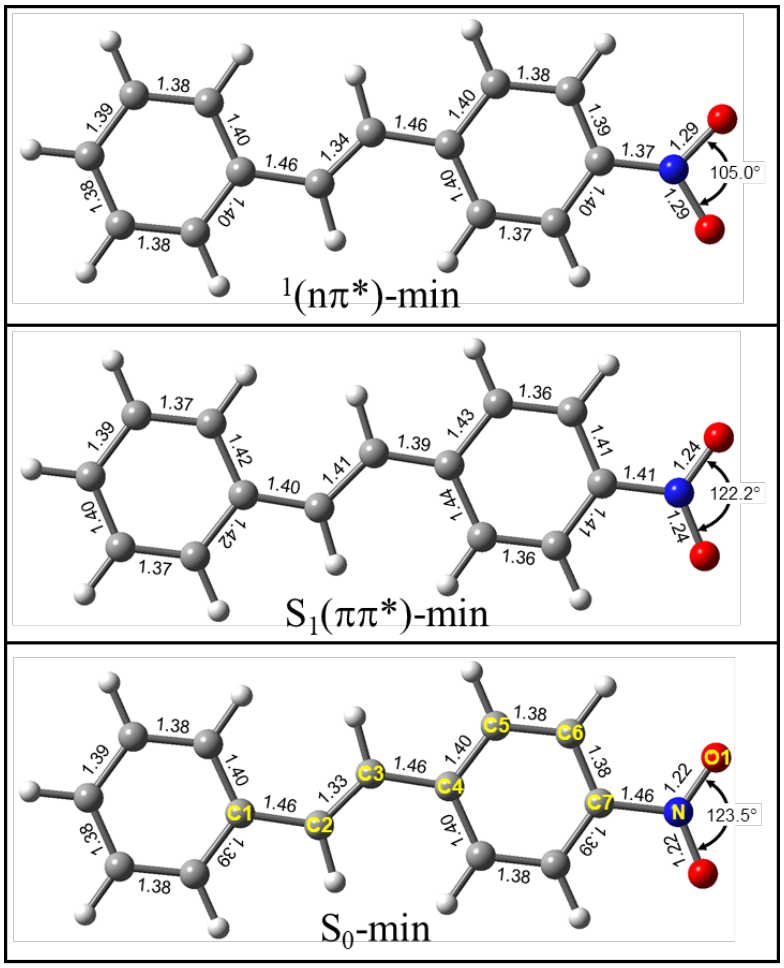

Fig. S6 Optimized structures of *t*-NSB (a) S_0 state, (b) $S_1(\pi\pi^*)$, and (c) $^1(n\pi^*)$ states in ACN calculated at levels of theory stated in the text. All atoms are essentially in the same plane. Important structural parameters (bond lengths in Å; bond angles in degree) are indicated.

at $S_1(\pi\pi^*)$-min structure

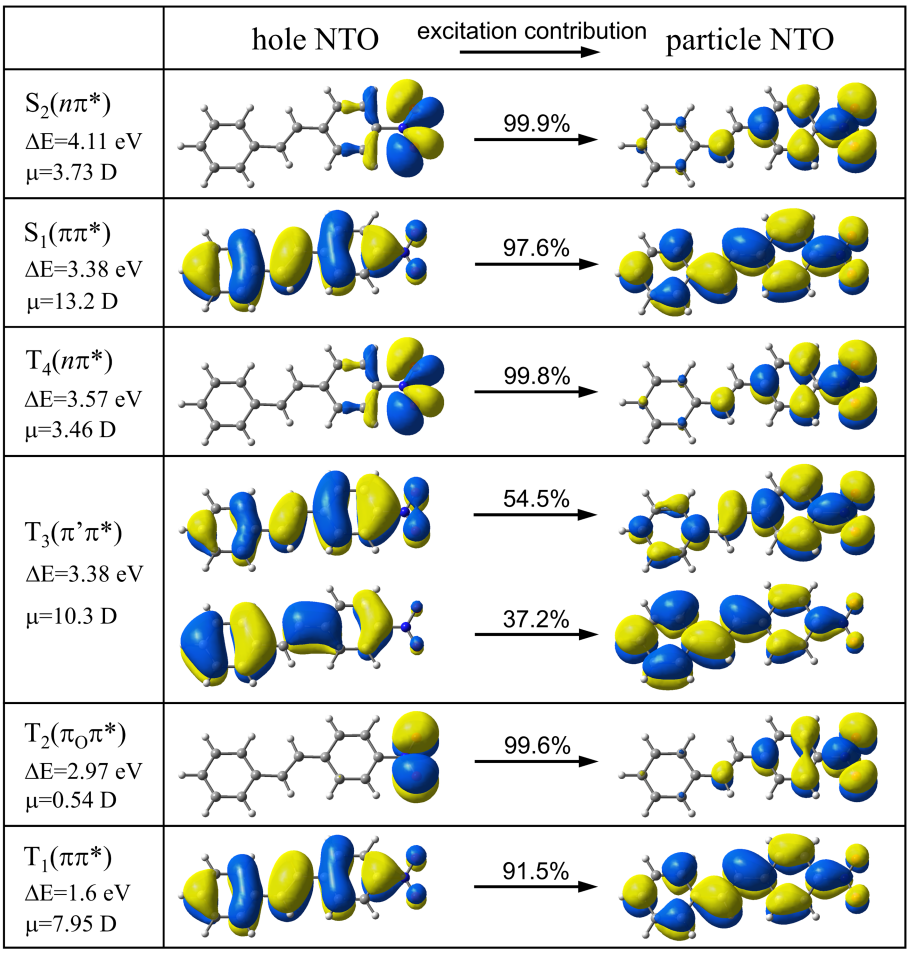

Fig. S7 Hole-particle pairs of NTOs (isosurface value=0.02 au) of several low-lying singlet and triplet states of *t*-NSB calculated at the $S_1(\pi\pi^*)$-min structure in CHX. Relative energy (ΔE) with respect to S_0-min and dipole moment (μ in Debye) of each state are also listed.

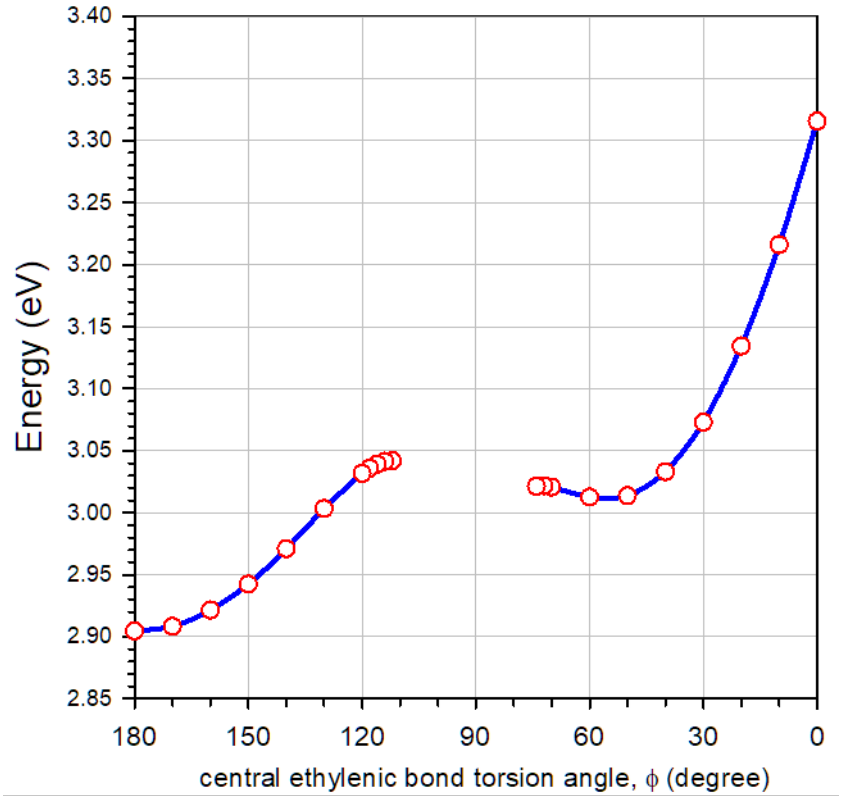

Fig. S8 Calculated S_1-state PE curves with respect to the S_0-min of SB along the S_1-MEP(ϕ) in ACN at the levels of theory stated in the text. S_1-MEP(ϕ) represents the S_1-state MEP of the dihedral angle ϕ(C1−C2−C3−C4) about the central ethylenic bond. The open circles are the calculated data, while the solid lines are interpolations of the calculated points.

References

1. Schmidt, B.; Laimgruber, S.; Zinth, W.; Gilch, P., A Broadband Kerr Shutter for Femtosecond Fluorescence Spectroscopy. *Applied Physics B-Lasers and Optics* **2003,** *76*, 809-814.
2. Arzhantsev, S.; Maroncelli, M., Design and Characterization of a Femtosecond Fluorescence Spectrometer Based on Optical Kerr Gating. *Appl. Spectrosc.* **2005,** *59*, 206-220.
3. Nakamura, R.; Kanematsu, Y., Femtosecond Spectral Snapshots Based on Electronic Optical Kerr Effect. *Rev. Sci. Instrum.* **2004,** *75*, 636-644.
4. Chiu, C. C.; Hung, C. C.; Chen, C. L.; Cheng, P. Y., Ultrafast Time-Resolved Broadband Fluorescence Studies of the Benzene-Tetracyanoethylene Complex: Solvation, Vibrational Relaxation, and Charge Recombination Dynamics. *J. Phys. Chem. B* **2013,** *117*, 9734-9756.
5. Lorenc, M.; Ziolek, M.; Naskrecki, R.; Karolczak, J.; Kubicki, J.; Maciejewski, A., Artifacts in femtosecond transient absorption spectroscopy. *Appl. Phys. B* **2002,** *74*, 19-27.
6. Gustavsson, T.; Cassara, L.; Gulbinas, V.; Gurzadyan, G.; Mialocq, J. C.; Pommeret, S.; Sorgius, M.; van der Meulen, P., Femtosecond Spectroscopic Study of Relaxation Processes of Three Amino-Substituted Coumarin Dyes in Methanol and Dimethyl Sulfoxide. *J. Phys. Chem. A* **1998,** *102*, 4229-4245.
7. Frisch, M. J.; Trucks, G. W.; Schlegel, H. B.; Scuseria, G. E.; Robb, M. A.; Cheeseman, J. R.; Scalmani, G.; Barone, V.; Petersson, G. A.; Nakatsuji, H.; *et al.*, *Gaussian 16, Revision B.01*. Gaussian, Inc.: Wallingford CT, 2016.